PROCEEDINGS OF SCIENCE

Time-dependent evolution of microquasar jets: First step towards exploring the role of jets in hard-soft state transitions

Dipankar Maitra*
Univ. of Amsterdam
E-mail: d.maitra@uva.nl

Sera Markoff
Univ. of Amsterdam
E-mail: s.b.markoff@uva.nl

Conventional steady-state jet models are not suitable for studying accretion outflows near state transitions in X-ray binary systems (XRB). Here, we present our ongoing work towards developing a time-dependent leptonic jet model to describe the soft-to-hard state transition in jets from X-ray binary systems. Taking into account the energetics of the co-evolving particle and photon distributions, we quantify the various cooling processes that seem to be relevant for microquasar (μQSO) jets. We study two extreme cases of shock acceleration, viz. (1) only one episode of shock acceleration at jet base, and (2) constant energy injection along the length of the jet. From these two cases we show that the observed flat radio–IR spectra seen in steady compact jets from XRBs in hard state cannot result from either a single acceleration episode or a constant rate of energy injection.

VII Microquasar Workshop: Microquasars and Beyond
September 1-5 2008
Foca, Izmir, Turkey

*Speaker.

PoS(MQW7)025

1. Introduction

Understanding the physical processes that lead to the observed complex instabilities in accretion flows near extremely compact objects such as black holes and neutron stars remains one of the most challenging problems in high energy astrophysics. Rapid transitions of the X-ray spectral energy distribution (SED) between almost completely nonthermal state (hard state) and almost completely thermal state (soft state), occurring in timescales of hours (or even faster) for accreting XRB systems, have been well observed over the past few decades. The timing properties of these systems also change remarkably during these state transitions. See e.g [13, 9, 17] for extensive reviews on observed spectral and timing properties of these states. One of the most exciting recent discoveries in this field has been the observation of jets and their strong association with the X-ray states (see e.g. [6] for a review). Typically, steady compact jets are seen when a source is in the hard state. But once the source makes a transition into the *soft* state, this steady, compact jet is not observed. Figure 1 schematically shows the path traced out by a *typical* X-ray transient, during the course of its outburst, on an X-ray colour-magnitude diagram.

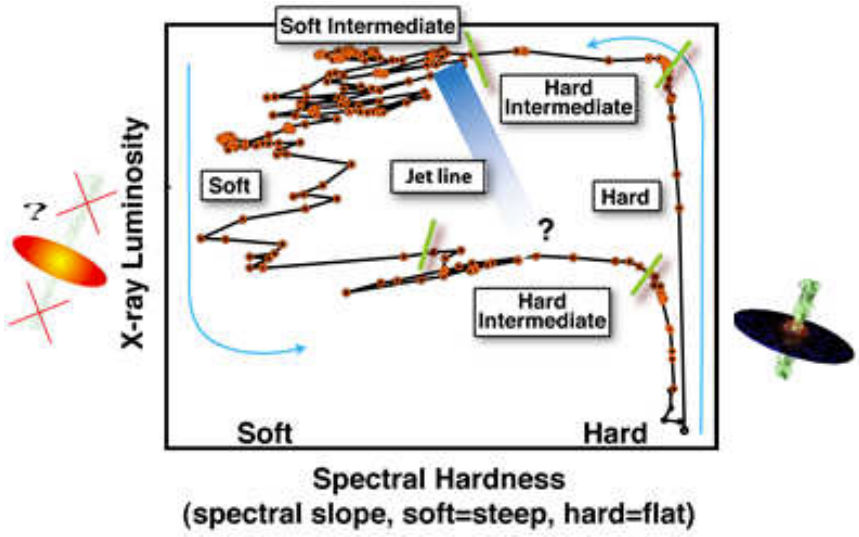

Figure 1: A schematic illustration showing the *typical* 'q'-shaped hysteresis loop traced by a transient X-ray binary system during the course of its outburst. Steady, compact jets characterized by flat radio–IR spectra are only seen in the *hard* state (on the right) but not in the *soft* state (on the left). The approximate region where steady jets seem to quench during the hard-to-soft transition is shown by the blue 'jet line'. Adapted from http://www.issibern.ch/teams/proaccretion/.

Here we present our ongoing work towards the development of a time-dependent jet model taking into account relevant physical processes. In §2 we present the building block of the jet-model, a one-zone model within which the continuity equation is solved to calculate the evolving particle energy distribution. Construction of the jet model and its application to two extreme cases of shock acceleration scenarios is described in §3. We discuss our results and avenues for future work in §4.

2. The one-zone "kernel" for electron cooling

In the one-zone model we initially assume that a homogeneous region of size ΔL contains a distribution of relativistic electrons $N(\gamma, t=0) = dN/d\gamma$, and is permeated by a tangled magnetic field B. We consider the following processes to influence the local evolution of the particle distribution within the jet:

- **Synchrotron cooling:** $\dot{\gamma}_{Syn} = 4\sigma_T c U_B \gamma^2/(3m_e c^2)$, where σ_T is the Thomson cross-section and $U_B = B^2/8\pi$ is the energy density of the magnetic field. Fitting observed data from μQSOs with steady state models ([11, 12]) suggest that beyond the shock, the characteristic virtual photon energy in the electron rest frame (assuming synchrotron radiation is Compton scattering of the virtual photons of the magnetic field) is much smaller than the electron rest mass energy, and hence the Thomson limit is applicable. Given the physical parameters in the jet, synchrotron cooling usually dominates all other cooling processes.

- **Inverse Compton (IC) cooling:** $\dot{\gamma}_{Com} = 4\sigma_{KN} c U_{rad}(\gamma,t)\gamma^2/(3m_e c^2)$, where σ_{KN} denotes the Klein-Nishina correction to the scattering cross-section, and $U_{rad}(\gamma,t)$ is the energy density of the radiation field. IC can be an important source of cooling especially near the base of the jet where photon energy densities are high.

- **Adiabatic expansion:** Following [16, 8], the cooling due to adiabatic expansion is taken to be of the form $\dot{\gamma}_{ad} = [\gamma/3V(t)]\partial V(t)/\partial t$. Here $(1/V)(\partial V(t)/\partial t)$ is the fractional rate of change of the volume of the source.

- **Particle escape:** We assume that particles can leak out of the source in a time scale $t_{esc} = \Delta L/c\beta$ where ΔL is the size of the source and β the bulk velocity of the jet plasma. Thus the change in the particle distribution due to particle escape is $[\partial N(\gamma,t)/\partial t]_{esc} = N(\gamma,t)/t_{esc}$.

- **Particle injection:** We further assume that particles can be injected into the source at a rate of $Q_{inj}(\gamma,t)$ cm^{-3} s^{-1}. The change in the particle distribution due to injection is $[\partial N(\gamma,t)/\partial t]_{inj} = Q_{inj}(\gamma,t)$.

Beyond the shock both the magnetic field as well as the particle densities decline monotonically outwards along the jet. The ratio of energy densities (both radiative as well as magnetic) to the size of the cell is quite small beyond the shock. Therefore we have neglected pair production/annihilation and synchrotron heating in the present version of the code.

Taking the above processes into account, the continuity equation describing the time evolution of the particle distribution is given by

$$\frac{\partial N(\gamma,t)}{\partial t} = \frac{\partial}{\partial \gamma}[\dot{\gamma}(\gamma,t)N(\gamma,t)] + Q_{inj}(\gamma,t) - \frac{N(\gamma,t)}{t_{esc}} \tag{2.1}$$

where $\dot{\gamma}(\gamma,t) = \dot{\gamma}_{Syn} + \dot{\gamma}_{Com} + \dot{\gamma}_{ad}$. Noting that the continuity equation above can be recast in the form of a Fokker-Planck equation, we used the fully implicit "Chang-Cooper algorithm" [2, 3] to solve it. The Chang-Cooper algorithm reduces the solution of the continuity equation to solving a tridiagonal system of equations. In our particular case, the absence of the synchrotron heating term (equivalent to the absence of the diffusion term in the Fokker-Planck equation) makes

the computations faster because the sub-diagonal vector in the tridiagonal system is identically zero. Furthermore, the Chang-Cooper algorithm conserves particles, ensures non-negativity and converges faster towards stable solutions.

Once the time-evolved particle distribution solution is obtained, we then compute the emitted spectral energy distribution (SED) due to angle averaged synchrotron emission for relativistic electrons [14]. Thereafter inverse Compton (IC) emission is computed incorporating Klein-Nishina correction for scattering beyond Thomson limit following the prescription of [1]. The seed photons for IC are the photons produced locally by synchrotron emission (synchrotron self-Compton; SSC) and also an external photon field (external Compton; EC). In our case, a source of seed EC photons could be the soft photon field produced by the accretion disk and/or the donor star. For simple cases with a constant power law injection, constant escape time, and no EC, we tested our code to reproduce the analytic solutions given e.g. by [10]. In Figure 2 we show the cooling of the high energy electrons, and the corresponding change in the SED at the source. In Figure 3 we show the appearance of the characteristic break in the particle distribution. In both cases we find excellent agreement with the analytic results (see e.g. [10]).

Since the motivation for the one zone model is to incorporate it within a jet framework, we can also assign a relativistic bulk velocity to the box. In this case we first compute the Doppler factor $D = [\Gamma(1-\beta cos\theta)]^{-1}$, where θ is the angle between velocity and line of sight, $\mathbf{c}\beta$ is the velocity, and $\Gamma = 1/\sqrt{1-\beta^2}$ is the bulk Lorentz factor. Then the observed SED is calculated by applying

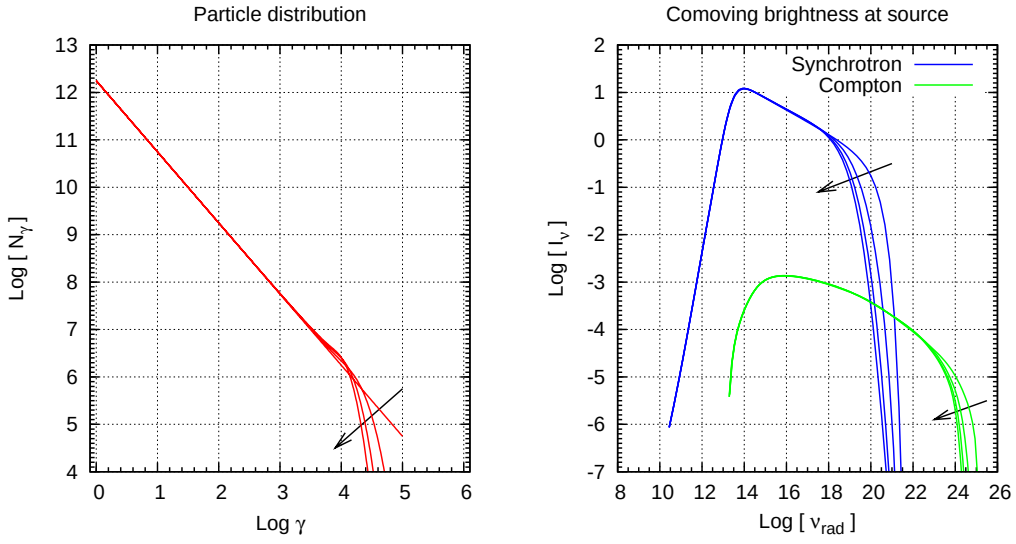

Figure 2: An example showing the cooling of the high-energy electrons and their effect on the broadband spectral energy distribution. The initial parameters for this run were: $B = 10^4$ Gauss, $R = 1.2 \times 10^8$ cm, $t_{esc} = 3 \times 10^{-3}$ s, $Q_{inj} \sim \gamma^{-1.5}$. The particle distributions are shown on the left panel. The synchrotron emission is shown by blue lines on the right panel and the inverse Compton (synchrotron self-Compton) component in the green. The arrows show the direction in which the distributions and SEDs evolve as time progresses; for $t/(10^{-8}\,\mathrm{s}) = 0, 3, 7$ and 1.

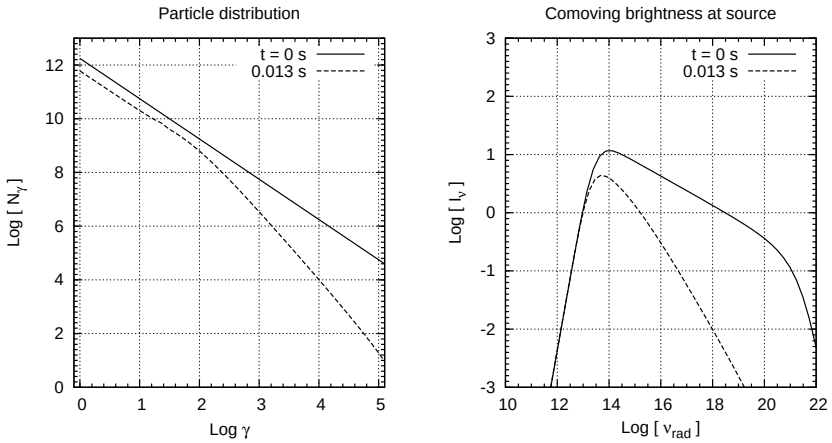

Figure 3: An example showing the "cooling break", with the same initial parameters as in Figure 2. The initial power law electron distribution is shown by the solid line on the left panel, and the corresponding spectral energy distribution shown on the right panel, also by a solid line. The optically thin region has a spectral index of -0.25 as expected theoretically. The dashed line on the left panel shows the particle distribution after 0.013 s ($\sim 4t_{esc}$), which clearly shows the cooling break at $log(\gamma) \sim 2.2$, consistent with analytic calculation ($\gamma_b \sim 3m_e c/4\sigma_T[U_B + U_{rad}]t$). The corresponding SED is shown by the dashed line on the right panel which also shows the characteristic extra steepening of the spectral index by 0.5.

the appropriate transformations of the emitted frequency and flux. As an example, in Figure 4 we show the particle distribution in a zone, the corresponding comoving brightness from the various components at the source and also the SED as seen from the Earth.

3. The *multi-zone* model of the jet

The observed spectrum from the compact jet is modeled as the sum of emission from cylindrical segments along the jet axis. The positions of these segments are static w.r.t the central compact object (and also the observer). Thus each of these segments radiates and cools as a one-zone box described in the previous section. We assume a symmetric geometry where the jet axis is parallel to the accretion disk normal. As the jet plasma flows outward from the central compact object it accelerates longitudinally through its pressure gradient and expands laterally with the sound speed [4, 5]. The velocity profile is obtained by solving the relativistic Euler equation. This in turn gives the radius of the segments and also the magnetic field as a function of distance along the jet axis.

As the particles (electrons) enter the jet we assume that they have a power law energy distribution of the form $N(\gamma) = dN/d\gamma = N_o\gamma^{-p}$ for $\gamma_{min} \leq \gamma \leq \gamma_{max}$ and $N(\gamma) = 0$ otherwise. In the context of steady state jet models ([11, 12]) this means that we are only considering the regions beyond the point where shock acceleration starts. As a starting point of our time-dependent model, we therefore take the relevant values (e.g. radius, velocity profile, number density, magnetic field strength) obtained from fitting observed data for the galactic black hole candidate GX 339–4 using the steady state model ([12]). The particle distribution within any single zone evolves according

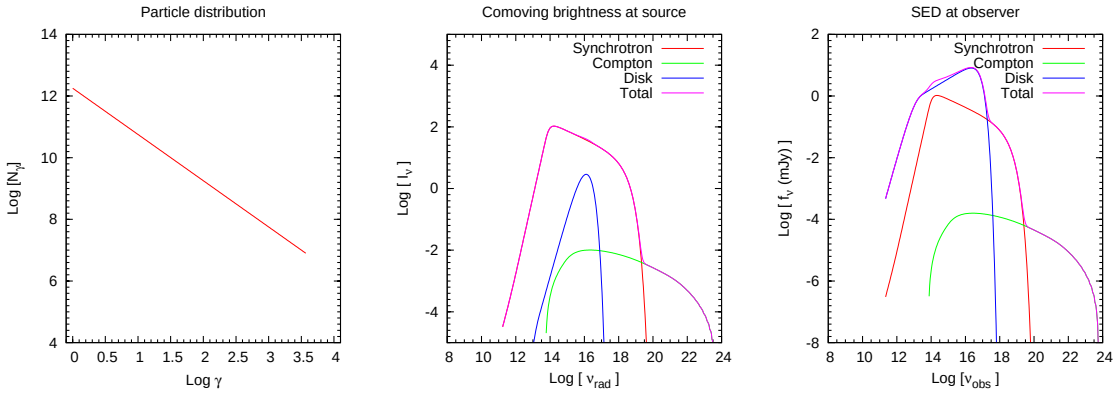

Figure 4: An example showing the emission from various radiative components in a one-zone model. The magnetic field strength is 6.1×10^4 Gauss. This zone is at a distance of $\sim 400\ R_g$ away from a central compact object of 7 solar mass. The zone has a bulk velocity $\beta\Gamma = 1.5$ and an inclination of 47 degrees w.r.t the line of sight (the numbers were taken from fitting broadband data from GX 339–4 using a steady state jet model [12]). In our model the system is at a distance of 6 kpc from Earth. We also include an additional photon field from a standard "Shakura-Sunyaev" accretion disk [15] with $T \sim R^{-3/4}$ radial temperature profile. The accretion disk parameters are: $T_{in} = 0.1\ keV$, $R_{in} = 100\ R_g$ and $R_{out} = 10^7\ R_g$. **Left panel:** The particle distribution in the zone. **Middle panel:** The comoving brightness at the source. The contribution from the synchrotron component is shown in red, inverse Compton in green, the photon field from the accretion disk in blue and the total spectrum in magenta. **Right panel:** SED observed from Earth. The colour scheme is the same as in the middle panel.

to equation 2.1 for a time $\Delta t = \Delta L/c\beta$, where ΔL is the length of the cylinder that constitutes the segment and β is the bulk velocity of the flow in this segment. Δt is also equal to the escape time (t_{esc}) during which the particles are convected from one segment to the next farther segment [7].

Using this model for emission from jets, and assuming a constant rate at which plasma enters the jet, we tested two extreme shock acceleration scenarios:

(1) Only one single shock redistributes particles into a power law as the plasma enters the jet. There is no extra particle injection along the jet ($Q_{inj} = 0$). The results are shown in Figure 5 where we show the observed SED from the various zones and also the summed overall spectrum. It is clear from the plot that for single episode of shock acceleration, the jet plasma cools too quickly and cannot reproduce the flat spectrum seen in steady compact jets from compact sources.

(2) We tested the other extreme case, where a constant injection rate per unit volume is assumed for every jet segment. Physically this could be interpreted as some form of distributed shock over the length of the jet. The injection function has the form $Q_{inj}(\gamma) = Q_o \gamma^{-1.5}\, H(\gamma; 1, 10^4)$ where $H(x, x_0, x_1) = 1$ for $x_0 \leq x \leq x_1$ and 0 otherwise. The normalization Q_o is adjusted so that the injection luminosity $L_{inj} = \int_{\gamma_{min}}^{\gamma_{max}} \gamma m_e c^2 Q_{inj}(\gamma) d\gamma = 10^{-6} L_{Edd}$ is constant for every segment of the jet. The results of this run are shown in Figure 6. Immediately after the plasma enters the jet, the cooling is dominant and for the first five zones the particle distribution cools rapidly as in case (1). The effect of this cooling moves the peak of the SED towards lower energy and lower brightness, as shown by the blue curves in Figure 6. However as the distribution cools, the typical cooling

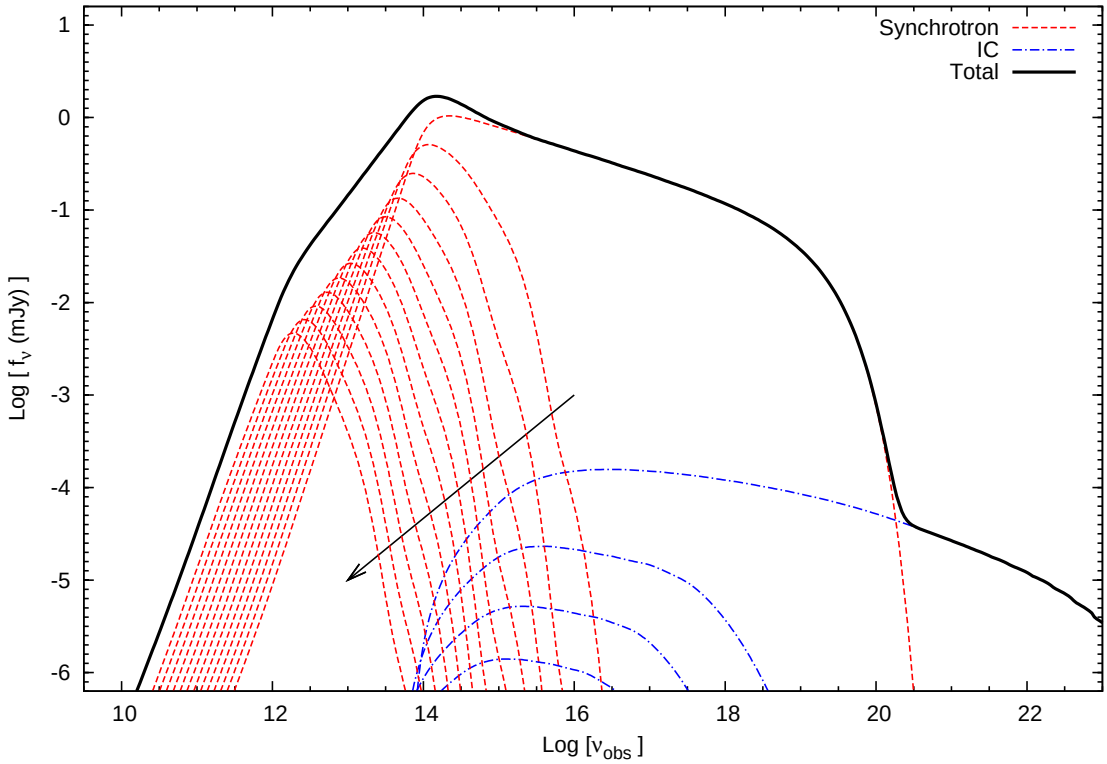

Figure 5: Observed SED from a jet with only one shock acceleration episode and $Q_{inj} = 0$. The observed synchrotron SED from the different zones are shown by red dashed lines. The corresponding IC spectra are shown by blue dash-dotted lines. The thick black line is the total emission as observed from the Earth. The arrow points in the direction of zones with increasing distance from the central compact object. The initial parameters (where the plasma enters the jet) used for this run were: Black hole mass= 7 Solar mass, $B_o = 5.5 \times 10^5$ Gauss, radius $= 33\ R_g$, number density$= 1.8 \times 10^{14}$. The initial particle distribution has the form of a power law of slope -1.5. For simplicity the accretion disk is turned off. The distance to the system is taken to be 6 kpc. From the plot it is clear that for a single acceleration episode, the particles cool down too quickly and do not reproduce the flat spectrum observed in the radio–IR from steady compact jets from compact sources..

time increases. Since the injection luminosity is constant, this implies that the actual amount of energy injected in the zones, within the cooling time becomes increasingly larger. As a result the particle distribution becomes dominated by injection and the resulting SEDs from the outer zones start getting increasingly brighter. This shows that a constant rate of injection along the length of the jet is also unlikely to produce the observed flat radio–IR spectra.

4. Discussion

We have developed the first steps towards a fully time-dependent model for jets from X-ray binaries by taking into account the relevant cooling and injection mechanisms. Preliminary runs of

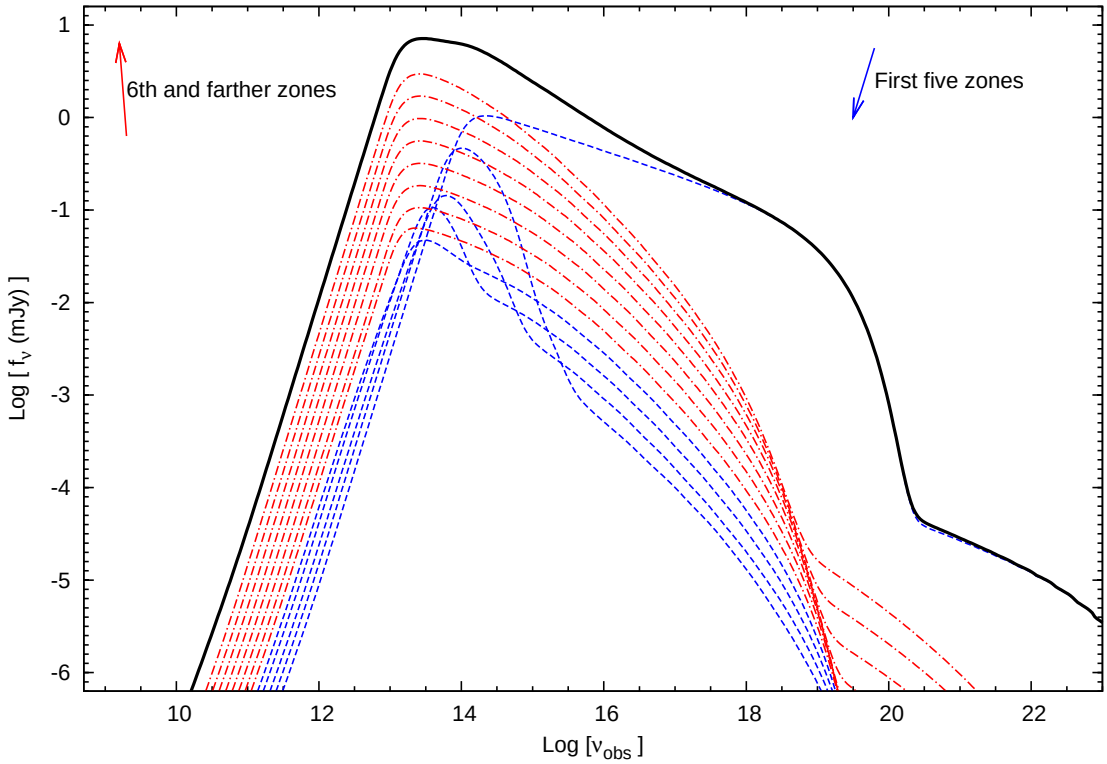

Figure 6: Observed SED from a jet with a constant injection $Q_{inj} = Q_o \gamma^{-1.5}$ for $1 \leq \gamma \leq 10^4$ and an injection luminosity of $10^{-6}\ L_{Edd}$. The remaining initial parameters are the same as in Figure 5. For simplicity, we show the total (synchrotron + IC) emission from the zones, and not the individual components. For the first five zones, shown by blue dashed lines, the particle distribution cools as in Figure 5. Consequently the peak of the SED moves towards lower energy and becomes fainter as shown by the direction of the blue arrow at top right. From the 6th zone onwards, shown by red dash-dotted line, the cooling time scale becomes so large that the energy injection rate begins to overcome the cooling. As a result the peaks of the SEDs start becoming increasingly brighter as shown by the direction of the red arrow. This catastrophic scenario is also unable to reproduce the flat radio–IR spectrum.

the model aimed towards understanding the importance of shock acceleration mechanism confirm that:

- Particles redistributed into a power law energy distribution by a single episode of shock acceleration will cool down rapidly. This will lead to a rather steep ($f_\nu \sim \nu^\alpha\ ; \alpha \gg 0$) SED, and large underprediction of radio flux compared to what is observed from X-ray binaries in the hard state.

- On the other hand, a constant energy injection per unit volume along the length of the jet, even at a small rate of $10^{-6}\ L_{Edd}$, leads to a steeply inverted spectrum ($f_\nu \sim \nu^\alpha\ ; \alpha \ll 0$) and overpredicts the radio flux.

At present the model incorporates cooling due to synchrotron, inverse Compton and adiabatic losses. Comparing steady state models of jets with observed data, these processes seem to be most dominant in compact jets from X-ray binaries. However this is true only beyond the "shock acceleration point", where particles are redistributed into a power law energy distribution. Closer to the central compact object, the energy densities are higher and other cooling processes such as pair production/annihilation can become important. We plan to include such processes within the model so that their contribution can be estimated when relevant. Also, we plan to incorporate synchrotron heating since the magnetic compactness can become quite high in certain circumstances, particularly near the base of the jet. As of now, the treatment of synchrotron emission is appropriate for relativistic electrons only (e.g. as in [14]). However since most of the particle energy distributions tend to peak at the lowest energies, we will incorporate a better treatment of the cyclo-synchrotron regime.

The model, written in C, is portable across a wide range of platforms. Once ready, the code will be made *open source*. It will be ported to be used within standard spectroscopic analysis software for the community to model broadband multi-wavelength data obtained from various missions. The present goal of the model is to study the quenching of jets during hard-to-soft transition in XRB systems. However with the advent of new missions like *Fermi*, and the increasing feasibility of coordinated simultaneous broadband observations of high energy sources, the model has a broad range of applicability from stellar black hole/neutron star jets to blazars.

Acknowledgments

This work was supported mainly by the Netherlands Organisation for Scientific Research (NWO) grant number 614000530. DM would also like to thank the Leids Kerkhoven-Bosscha Fonds (LKBF) for travel grant 08-296. It is a pleasure to acknowledge the warm hospitality of the LOC.

References

[1] Blumenthal, G. R., & Gould, R. J. 1970, Reviews of Modern Physics, 42, 237

[2] Chang, J. S., & Cooper, G. 1970, Journal of Computational Physics, 6, 1

[3] Chiaberge, M., & Ghisellini, G. 1999, MNRAS, 306, 551

[4] Falcke, H. 1996, ApJ, 464, L67

[5] Falcke, H., & Markoff, S. 2000, A&A, 362, 113

[6] Fender, R. 2006, in Compact stellar X-ray sources. Edited by Walter Lewin & Michiel van der Klis. Cambridge Astrophysics Series, No. 39., p. 381–419

[7] Graff, P. B., Georganopoulos, M., Perlman, E. S., & Kazanas, D. 2008, arXiv:0808.2135

[8] Gupta, S., & Böttcher, M. 2006, ApJ, 650, L123

[9] Homan, J., & Belloni, T. 2005, Ap&SS, 300, 107

[10] Kardashev, N. S. 1962, Soviet Astronomy, 6, 317

[11] Markoff, S., Nowak, M. A., & Wilms, J. 2005, ApJ, 635, 1203

[12] Maitra, D. Markoff, S., Brocksopp, C., Noble, M., Nowak, M. A., & Wilms, J. 2008, submitted to MNRAS

[13] McClintock, J. E., & Remillard, R. A. 2006, in Compact stellar X-ray sources. Edited by Walter Lewin & Michiel van der Klis. Cambridge Astrophysics Series, No. 39., p. 157–213

[14] Rybicki, G. B., & Lightman, A. P. 1979, New York, Wiley-Interscience

[15] Shakura, N. I., & Syunyaev, R. A. 1973, A&A, 24, 337

[16] Sikora, M., Błażejowski, M., Begelman, M. C., & Moderski, R. 2001, ApJ, 554, 1

[17] van der Klis, M. 2006, in Compact stellar X-ray sources. Edited by Walter Lewin & Michiel van der Klis. Cambridge Astrophysics Series, No. 39., p. 39–112